Exploring the Limitation of Molecular Water Oxidation Catalysts

Busch, Michael ; Fabrizio, Alberto ; Luber, Sandra ; Hutter, Jürg ; Corminboeuf, Clemence

Abstract: Linear free energy scaling relationships (LFESRs) and volcano plots are routinely used to assess the performance of heterogeneous electrocatalysts and have only recently been concretely exploited in homogeneous catalysis. These tools efficiently compare and provide a global evaluation of catalyst performance while highlighting the limitations for a given reaction. In the framework of solid-state water oxidation, a minimal overpotential of 0.4 eV has been predicted on the basis of LFESRs. Considering the very different nature of homogeneous catalysts compared to solid-state systems, the validity of scaling relationships determined for the former cannot be assumed. To evaluate the global limitations of molecular O-2 evolution catalysts, LFESRs are established for all key intermediates for different metal (Mn, Co, Ru, Rh, Ir) and ligand (corrole and perfluoro-porphyrin) combinations assuming a mononuclear mechanism that proceeds through *=OH, *=O, and *-OOH intermediates. Our computations indicate that the LFESRs strongly depend on the choice of density functional. Using GMC-QDPT2 as a benchmark, strong scaling relationships between all intermediates are observed, but the relationships between *-OH and *=O significantly differ from those found in solid-state systems. Consequently, the shape of the molecular volcano plot changes drastically from its solid-state counterpart and shows a broad plateau at the top where the overpotential is nearly independent of the choice of catalyst. This plateau renders the performance of molecular catalysts extremely robust, but inhibits improvements by proceeding through alternative reaction mechanisms.

DOI: https://doi.org/10.1021/acs.jpcc.8b03935

THE JOURNAL OF PHYSICAL CHEMISTRY C

Article

Cite This: J. Phys. Chem. C 2018, 122, 12404−12412

pubs.acs.org/JPCC

Exploring the Limitation of Molecular Water Oxidation Catalysts

Michael Busch,[†,‡,⊥] Alberto Fabrizio,[†,‡,⊥] Sandra Luber,[§,∥] Jürg Hutter,[§,∥] and Clemence Corminboeuf*[,†,‡]

[†]Laboratory for Computational Molecular Design, Institute of Chemical Sciences and Engineering and [‡]National Centre for Computational Design and Discovery of Novel Materials (MARVEL), École Polytechnique Fédérale de Lausanne, 1015 Lausanne, Switzerland

[§]Department of Chemistry and [∥]National Centre for Computational Design and Discovery of Novel Materials (MARVEL), University of Zürich, 8057 Zürich, Switzerland

Supporting Information

ABSTRACT: Linear free energy scaling relationships (LFESRs) and volcano plots are routinely used to assess the performance of heterogeneous electrocatalysts and have only recently been concretely exploited in homogeneous catalysis. These tools efficiently compare and provide a global evaluation of catalyst performance while highlighting the limitations for a given reaction. In the framework of solid-state water oxidation, a minimal overpotential of 0.4 eV has been predicted on the basis of LFESRs. Considering the very different nature of homogeneous catalysts compared to solid-state systems, the validity of scaling relationships determined for the former cannot be assumed. To evaluate the global limitations of molecular O_2 evolution catalysts, LFESRs are established for all key intermediates for different metal (Mn, Co, Ru, Rh, Ir) and ligand (corrole and perfluoro-porphyrin) combinations assuming a mononuclear mechanism that proceeds through *−OH, *═O, and *−OOH intermediates. Our computations indicate that the LFESRs strongly depend on the choice of density functional. Using GMC-QDPT2 as a benchmark, strong scaling relationships between all intermediates are observed, but the relationships between *−OH and *═O significantly differ from those found in solid-state systems. Consequently, the shape of the molecular volcano plot changes drastically from its solid-state counterpart and shows a broad plateau at the top where the overpotential is nearly independent of the choice of catalyst. This plateau renders the performance of molecular catalysts extremely robust, but inhibits improvements by proceeding through alternative reaction mechanisms.

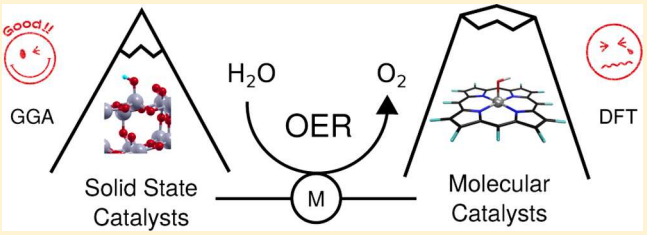

INTRODUCTION

The conversion of surplus electricity from renewable sources into fuels is a key process in achieving a sustainable society. Energy can be stored either through the electrochemical/photochemical generation of H_2[1−3] or by reducing CO_2,[4−9] each process of which are, unavoidably, coupled with the oxidation of water to O_2.[1,2,10] On an industrial scale, water splitting is facilitated within alkaline or proton-exchange membrane (PEM) electrolyzers. The former make use of cost-effective non-noble electrocatalysts. However, these electrolyzers suffer from a significantly lower current density and problems arising from the migration of products through the diaphragm that separates the anode and the cathode. This not only reduces the purity of the H_2 and O_2 products, but also represents a potential safety hazard.[1] PEM electrolyzers, on the contrary, operate under very acidic conditions that allow proton transfer through the Nafion membrane that separates the electrodes. The good proton conductivity of Nafion allows significantly higher current densities, but the low pH limits the choice of catalysts.[1] In state-of-the-art PEM electrolyzers, the oxygen evolution reaction (OER) is catalyzed by dimensionally stable anodes,[10] which contain mixtures of Ir, Ru, and Ti oxides that provide enhanced stability (up to 10 years) even under the harsh conditions present in industrial electrolysis.[10]

Alternative to industrial OER catalysis, nature has its own mechanism for accomplishing water oxidation. Plants efficiently catalyze this reaction within photosystem II (PS II) using an enzyme active site that consists of a $CaMn_4O_x$ tetramer.[11−14] Not surprisingly, PS II has served as inspiration for numerous molecular water oxidation catalysts that have been successfully synthesized. The field was pioneered with the development of Meyer's blue dimer,[15] a Ru dimer terminated by ter-pyridine ligands. Numerous alternative molecular catalysts now exist, based on, for example, Ir,[16−18] Ru,[18−20] as well as earth-abundant transition metals like Co,[18,21−23] Mn,[18,24−30] Fe,[31−37] Ni,[38−41] and Cu.[42−44] Interestingly, most of these metals also show high activity when the OER is catalyzed by heterogeneous species.[18,30,45−55] One key restriction on the large-scale applicability of molecular OER catalysts is their significantly lower stability compared to that of traditional solid-state catalysts.[25,56] However, the possibility of fine-tuning the activity

Received: April 26, 2018
Published: May 18, 2018

DOI: 10.1021/acs.jpcc.8b03935
J. Phys. Chem. C 2018, 122, 12404−12412

of the metal core by exchanging ligands offers a promising route for molecular catalysts that is not easily accessible for heterogeneous species. Proceeding in this manner may allow the activity of molecular catalysts to surpass their solid-state counterparts.

In the following, we provide the first general picture of the performance of molecular OER catalysts by computing their overpotential. This general overview is obtained from linear free energy scaling relationships (LFESRs),[57−59] which summarize the relative stability of key intermediates with respect to a single descriptor. On the basis of these relationships, global overpotential limitations can be extracted and visualized as a volcano plot.[60−62] Catalysts displaying the best possible performance for a given reaction mechanism appear at or near the top of the volcano and fulfill Sabatier's principle,[63,64] as also invoked by Shaik et al. (within the context of the energy span model[65,66]), Swiegers et al.,[67] and our group[58] for homogeneous catalysis. In the case of unfavorable LFESRs, this top can be far from the hypothetical "ideal performance" that would be achieved if all reaction steps possessed equivalent reaction energies.[47,58,68] In computational electrochemistry, typically only the thermodynamic limitations are included in volcano plots, in contrast to the kinetic volcano plots that have recently appeared in the literature for homogeneous catalysis.[69] The simpler thermodynamic volcanoes represent a best-case scenario where catalysts appearing on the top may still be hindered by poor kinetics. However, catalysts falling far from the top can be excluded as even low activation barriers will not aid in overcoming a significant thermodynamic barrier. Similarly, a volcano top placed far below the ideal case will not benefit significantly from favorable kinetics.

Solid-state OER catalysts are generally analyzed using a volcano plot representative of a mononuclear mechanism that proceeds through *−OH, *═O, and *−OOH intermediates. Overall, a strong linear scaling relationship exists between the *−OH and *−OOH intermediates.[47,68] Specifically, the difference in the surface adsorption energy between these intermediates (i.e., the intercept) is 3.2 eV, which holds independent of the choice of catalyst (ranging from oxides[47] to transition metal-doped graphenes[70,71]) required for this $2e^-/H^+$ oxidation step. This strong scaling relationship translates into a minimal overpotential of 0.4 eV.[47,68] Considering the very different nature of a single transition metal coordinated by a versatile set of ligands present in molecular systems, the existence of the same scaling relationship seen in solid-state catalysts cannot be assumed. The purpose of this work is to establish the LFESRs and provide the corresponding global limitations for a test set of homogeneous transition metal catalysts coordinated by corrole and porphyrin ligands. Comparable systems have been individually considered experimentally as potential molecular OER catalysts.[72,73] To ensure the robustness of the scaling relationships, results from different density functionals are compared with highly accurate multiconfiguration computations. On the basis of these reference computations, reliable LFESRs are extracted and cast into a volcano plot that identifies the global limitations of molecular OER catalysts.

■ COMPUTATIONAL METHODS

The geometries of the four key intermediates (*−OH_2, *−OH, *−OOH, and *═O) for each compound in the test set were optimized at the TPSS[74]-D3[75]/def2-SVP level, including the use of effective core potentials[76] for Ru, Rh, and Ir. Solvation effects were accounted for using the IEFPCM[77,78] implicit solvent model for water. The relative stability of different spin states was evaluated for each compound at the same theoretical level. Each of the electrochemical potentials were computed using Rossmeisl's theoretical normal hydrogen electrode,[79,80] which converts electronic energies to Gibbs free energies through a constant set of entropy and zero-point energy corrections. Basis set dependence of the LFESRs was found to be negligible (Supporting Information).

Linear scaling relationships were constructed for a set of 20 qualitatively different density functional approximations at the TPSS-D3 geometries. Each selected functional presents specific advantages over the others for treating the thermochemistry of metal-oxo porphyrins and corroles. The generalized gradient approximation (GGA) and meta-GGA functionals partially capture static correlation effects as a result of an advantageous error cancellation.[81] The electronic structure of transition metal complexes, often characterized by high-spin polarized metal sites, makes them sensitive to the correct treatment of static correlation. Chemically speaking, a failure to include this type of electron correlation leads to a dramatic overestimation of the ionic character of metal−ligand bonds. In this work, five GGA functionals (B97-D,[82] BLYP,[83,84] BP86,[83,85] BPBE,[83,86,87] and PBE[86,87]) and two meta-GGAs (TPSS[74] and M06L[88]) were included. The presence of a fixed percentage of exact exchange in global hybrids and meta-GGA hybrids leads to a significant reduction of the delocalization error (DE), which is an additional shortcoming of density functional approximations. This work includes six global hybrids featuring increasing percentages of exact exchange (B3LYP,[84,89,90] B3PW91,[84,91] mPW3PBE,[86,87,92] APFD,[93] PBE0,[94,95] and BHHLYP[96]) and four meta-GGA hybrids (M06,[97] BMK,[98] M06-2X,[97] and M06-HF[99,100]).

Finally, long-range-corrected and range-separated hybrids retrieve the correct long-range behavior of the exchange−correlation potential, which reduces the DE even more effectively than in global hybrids. Here, the most commonly used functionals from this last class (LC-ωPBE,[101−103] ωB97X-D,[104] and CAM-B3LYP.[105]) have been selected. All density functional computations were performed in Gaussian 09, revision D.01[106] with the same basis set and effective core potentials as for TPSS. Benchmark computations were performed using the general multiconfiguration quasi-degenerate perturbation theory (GMC-QDPT2)[107,108] and the def2-SVP basis set using GAMESS-US.[109] For additional computational details, see the Supporting Information.

Model Systems. This work assumes the OER to proceed through the mononuclear mechanism (involving a series of *−OH, *═O, and *−OOH intermediates), allowing a direct comparison between state-of-the- art solid-state OER catalysts[79,80] and their molecular counterparts. Connections to alternative mechanisms are discussed later (vide infra). Note that the intrinsic limitations associated with a thermodynamic-only picture did not affect the resulting volcano plots, as the general conclusions hold thanks to Brønstedt−Evans−Polanyi relationships.[69,110] A test set of eight neutrally charged systems consisting of Mn, Co, Ru, and Rh embedded into perfluoroporphyrin ($PorphF_{12}$) and Co, Ru, Rh, and Ir coordinated to corrole ($CorrH_{11}$) was used (Figure 1). Accordingly, the formal oxidation states of metal ions in $PorphF_{12}$ varied between +II (*−OH_2), +III (*−OH and *−OOH), and +IV (*═O), whereas those in $CorrH_{11}$ were taken as +III (*−OH_2), +IV

DOI: 10.1021/acs.jpcc.8b03935
J. Phys. Chem. C 2018, 122, 12404−12412

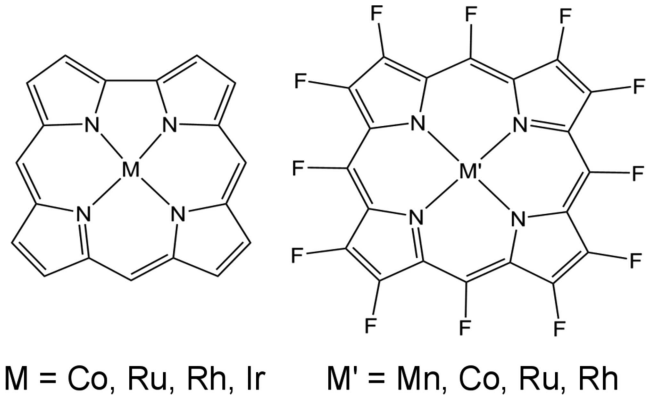

Figure 1. Schematic representation of the considered complexes.

(*−OH and *−OOH), and +V (*═O). The test systems were specifically chosen to cover a large range of binding energies, which increases the statistical robustness of our results. On the basis of the high R^2 values, the established relationships are statistically meaningful. Following convention,[47,68] LFESRs were established by plotting the *═O and *−OOH energies with respect to the *−OH reference state. LFESRs between *−OH and *−OOH were obtained both for freely varying slopes and, in accordance with previous work in solid-state electrochemistry, for a slope fixed at unity. The volcano plot was constructed assuming a *−OH/*−OOH scaling relationship with a slope fixed at 1. In contrast, no constraint was applied to the linear regression coefficients of the *−OH/*═O scaling relationship. The resulting volcano plot was then used to predict the overpotential of perfluoro-porphyrins of Fe, Ni, and Cu, solely based on the computation of the descriptor (ΔG(M−OH)). The corresponding scaling relationships governing the behavior of the heterogeneous catalysts were extracted from an extensive set of transition metal oxides[47,111] and transition metal-doped graphenes.[70] Full details regarding linear scaling relationships and the construction of volcano plot are given in the Supporting Information.

RESULTS AND DISCUSSION

Establishing Scaling Relationships. A complete description of the OER catalytic cycle that proceeds through a mononuclear mechanism requires determination of the scaling relationships between intermediates *−OH/*═O and *−OH/*−OOH. For solid-state catalysts, these relationships are known to be computationally robust, with different electronic structure methods[47,112,113] and the introduction of solvation effects[114] not affecting the general chemical conclusions on the composition of ideal catalysts.

This reassuring robustness, however, disappears for molecular catalysts. As shown in Figure 2, the solid-state LFESRs agree with previously published data,[47,68] whereas different theoretical levels result in markedly different LFESRs for the molecular catalysts. For the latter case, these methodological discrepancies profoundly impact the chemical conclusions drawn from the LFESRs. For instance, the low intercept of the *−OH/*−OOH scaling relationship using TPSS (2.4 eV), compared to solids (3.2 eV), implies that for molecular catalysts, the reaction could proceed at a negligible overpotential. On the contrary, this same conclusion is invalidated if conclusions are drawn using the LFESRs computed at the M06 level (intercept 3.2 eV). Given the fundamental disagreement of the chemical conclusions that are drawn from the TPSS and M06 computations, we recomputed the LFESRs of the model systems with 20 different density functionals, including representative hybrid and semilocal variants. A comparison of

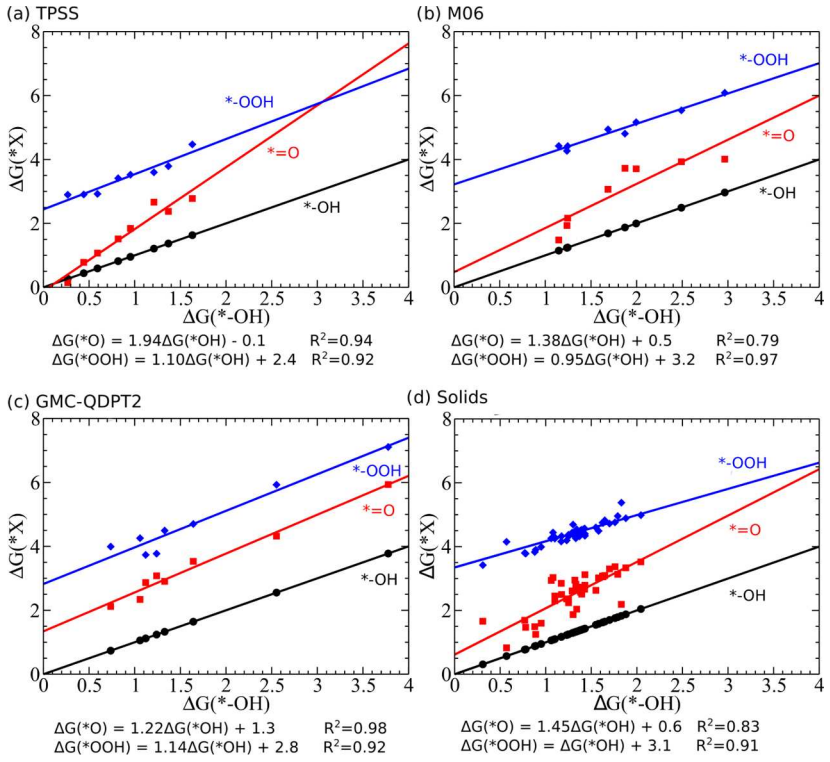

Figure 2. Linear free energy scaling relationships among the binding energies of *−OH, *═O, and *−OOH for molecular catalysts at (a) TPSS, (b) M06, and (c) GMC-QDPT2 levels of theory and for (d) solid-state catalysts. Solid-state data were taken from refs 47, 67, 108.

DOI: 10.1021/acs.jpcc.8b03935
J. Phys. Chem. C 2018, 122, 12404−12412

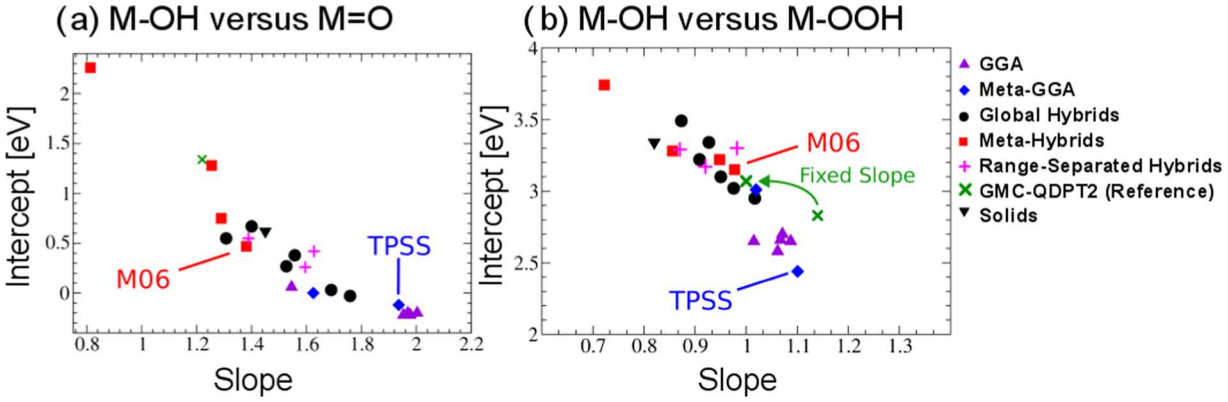

Figure 3. Summary of the (a) *−OH/*═O LFESR and (b) *−OH/*−OOH LFESR obtained for 20 different functionals. Each LFESR is obtained from a test set comprising eight data points.

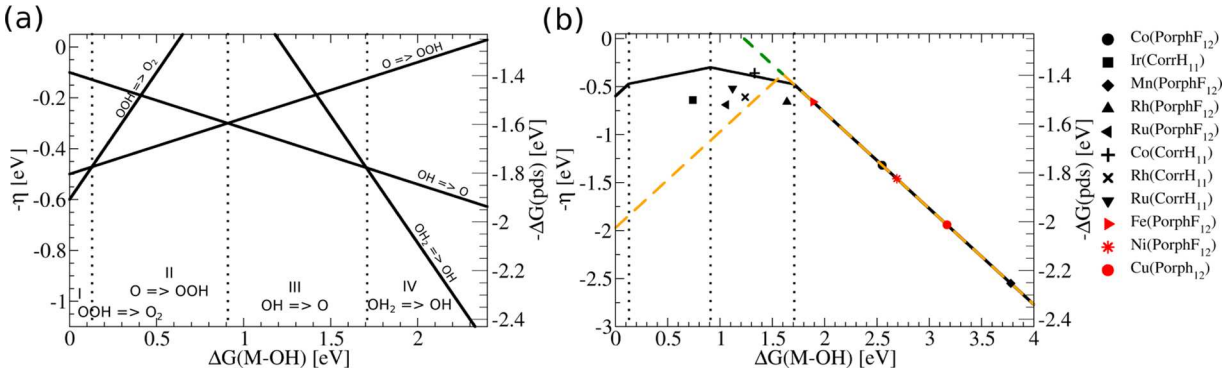

Figure 4. a) Overview of the thermodynamics of water oxidation to O_2 as derived from the linear free energy scaling relationships of Figure 2c at the GMC-QDPT2 level. (b) Volcano plot, η corresponds to the overpotential and ΔG(pds) corresponds to the redox potential of the potential determining step ($\eta = \Delta G(\text{pds}) - 1.23$ eV). For the scaling between *−OH and *−OOH, a slope of 1 was assumed. Molecular volcano plot, black lines; solid-state volcano plot for a mononuclear mechanism, orange dashed line. Improvements for solid-state catalysts through a bifunctional or binuclear mechanism (green dashed line). Black symbols correspond to the complexes used for the construction of the LFESRs, whereas in red are the complexes for which only the descriptor was computed.

the slopes and intercepts obtained for each different functional category is shown in Figure 3.

Benchmark values for the linear scaling relationships were obtained at the GMC-QDPT2 level and indicate strong scaling among all three intermediates, as attested to by the high R^2 values (Figure 2c). Accordingly, the significant amount of scatter produced by some functionals indicates they do not accurately describe the molecular OER intermediates. Comparing the DFT results and GMC-QDPT2 results further stresses the methodological challenges of constructing accurate molecular LFESRs.

From a chemical perspective, the benchmark computations provide a reliable comparison of homogeneous catalysts with their solid-state counterparts. In fact, the accurate computations show a slope close to unity for the LFESR between *−OH and *−OOH. If this slope is fixed at 1, a constant difference of 3.07 eV is observed for the $2H^+/e^-$ oxidation reaction, which agrees well with solid-state catalysts.[47,68] In contrast, the LFESR between *−OH and *═O has a slope of 1.22 and a high intercept of ∼1.3 eV, which deviates significantly from previously reported solid-state data as well as from most of the density functionals considered.

From a methodological perspective, the LFESRs are in most cases ordered by functional class. For instance, functionals without exact exchange generally yield near 2.7 eV for the *−OH/*−OOH scaling relationship, which is far below the reference values for both solid-state and our benchmark method. Thus, this low intercept represents a clear methodological artifact. The lone exception is the flexible (37 adjustable parameters) and extensively trained[88] M06L functional, which has a significantly higher intercept of 3.0 eV. Overall, this class of functionals tends (aside from M06L) to deviate from the GMC-QDPT2 reference data, which would lead to the erroneous conclusion that mononuclear OER catalysts should perform significantly better than would their solid-state counterparts.

In contrast, density functionals, including exact exchange, show a constant difference of ∼3 eV (or higher) between *−OH and *−OOH. For the *−OH/*═O intermediate, all categories of hybrid functionals result in LFESRs with slopes between 1.3 and 1.7 and low intercepts. Globally, functionals with lower percentages of exact exchange better recover the behavior seen in the solid-state LFESRs proposed by Koper et al.[68] and lie reasonably close to the GMC-QDPT2 reference.

The influence of different density functionals on individual binding energies follows the same trend as the LFESRs (see the Supporting Information). Specifically, semilocal functionals systematically overbind intermediates on the order of 1 eV compared to our benchmark computations. Hybrid functionals, on the contrary, generally underbind the catalytic intermediates, with the error decreasing when less exact exchange is included.

DOI: 10.1021/acs.jpcc.8b03935
J. Phys. Chem. C 2018, 122, 12404−12412

Generally, the poor performance of density functionals highlights the challenge of accurately modeling these metal-oxo intermediates using different electronic structure methods. Ultimately, the accuracy of each functional depends on its intrinsic ability capturing the subtle balance between the effects brought on by static correlation and the consequences of spurious electron delocalization.[115−119] Our findings show that none of the functionals we tested is able to account for both these drawbacks. Nevertheless, the noteworthy performance of hybrids, such as M06 and PBE0, indicates that this class of functionals is sufficiently reliable to establish molecular LFESRs for the OER. In cases where hybrid functionals are prohibitively expensive, only M06L is able to provide semiquantitative accuracy.

Implications for the OER. The information obtained from the LFESRs (as determined at the accurate GMC-QDPT2 level) can be cast into a volcano plot, which uncovers the general electrochemical performance limitations of molecular OER catalysts. Each of the reaction steps in the global reaction profile (Figure 4a) is constructed by plotting the redox potentials derived from the LFESRs as a function of the ΔG(M−OH) descriptor. The final volcano shape (Figure 4b) depicts only the most energetically costly steps. The changing nature of the energetically most difficult (i.e., potential determining) step naturally divides the volcano into four distinct regions. For catalysts with very strongly bound intermediates (i.e., those lying in region I, far left of Figure 4a), the release of O_2 through oxidation of *−OOH determines the overpotential. However, none of the molecular catalysts of the test set catalysts fall in this region. Destabilizing the intermediates either by choosing more reactive metals or by inclusion of suitable ligands shifts the catalysts into regions II and III. Here, either the O−O bond formation through nucleophilic attack at the *═O intermediate (region II) or the oxidation of *−OH to *═O (region III) determines the thermodynamic overpotential. Importantly, regions II and III constitute the top of the volcano plot, where the most active OER catalysts are found. An important aspect of the volcano plot is its generality with respect to changes in metal centers, oxidation states, spin states, or coordination geometry. Previous observations[70,120] have found that these factors do not influence the scaling relationships or the shape of the volcano. Instead, a change in one of these parameters simply results in a shift of the catalyst toward either weaker or strong binding. This new binding energy can then be used to predict the activity of the catalyst in its altered state using the same volcano plot.[70,120]

It is unsurprising that second- and third-row transition metals, such as Ru and Ir, appear at the top of the volcano in regions II and III because highly active molecular catalysts based on these metals are experimentally well known.[18] On the contrary, a catalyst incorporating a more earth-abundant metal, Co, also appears atop the volcano plot, but only when coupled with a corrole ligand. Replacing corrole with its perfluoro-porphyrin equivalent causes a shift toward the weak binding side of the volcano plot, where the oxidative adsorption of H_2O determines the overpotential (region IV). From a chemical perspective, Co represents a concrete example of how ligand choice can improve the catalytic efficiency of the metal center. Interestingly, it appears that second- and third-row transition metals are less influenced by their ligand, which appears as less pronounced changes in estimated overpotential for these species.

Robust LFESRs offer an overview of the global limitations of a catalytic process. For this reason, they are applicable not only to the compounds used for their construction, but also to any other prospective catalyst. For instance, the performances of perfluoro-porphyrins of Fe, Ni, and Cu (red symbols Figure 4b) have been assessed and added to the volcano plot solely by computing the descriptor (ΔG(M−OH)). Although the Fe complex has the lowest overpotential of the group (0.66 eV), all of these compounds fall on the weak binding volcano slope, which is characterized by rapidly increasing overpotentials (region IV). The fact that the Fe, Ni, and Cu porphyrin complexes do not fall on the top of the volcano plot aligns well with experimental evidence that these three metal ions are active only when two cis ligand sites are available for coordination.[31,40−42] Active water oxidation catalysts with only one labile ligand are known for Fe, but only when the metal adopts oxidation states between +III and +V.[36] In contrast, the oxidation states of the metals-porphyrins considered here vary between +II and +IV (see the Computational Methods).

Clearly, the volcano plot obtained for molecular systems differs significantly from that commonly accepted in heterogeneous electrocatalysis. The latter is characterized by only two potential determining steps, representing the formation of *−OOH from *═O and the oxidation of *−OH to *═O. These two restricting reactions meet in a peak at a *−OH binding energy of 1.6 eV and a minimal overpotential of 0.4 eV. In contrast, the molecular volcano plot is characterized by a broad plateau where species with binding energies [ΔG(M−OH)] between 0.1 and 1.7 eV have roughly similar overpotentials. The minimal overpotential for molecular catalysts is approximately 0.3 eV and, owing to the broad plateau, is almost independent of the choice of catalyst. Accordingly, this lower overpotential means that the best molecular OER catalysts should display higher activity relative to the ideal solid-state systems, assuming both processes follow the mononuclear mechanism. Additionally, the thermodynamic overpotential increases quickly for solid-state electrocatalysts, whereas it remains much more constant, even relatively far from the top of the volcano, for molecular systems. However, if one moves beyond this plateau region, a rapid drop in activity is expected.

On the basis of the results discussed above, it is tempting to propose that molecular OER catalysts should, at least from a purely thermodynamic perspective, be superior to solid-state catalysts. However, caution must be taken, as the above-discussed results only consider the mononuclear mechanism. Indeed, alternative pathways featuring, for example, binuclear[29,55,121] or bifunctional[52,70,122] components have also been discussed for water oxidation. Similar to the mononuclear mechanism, these alternative reaction paths each require the oxidation of water to *═O. After formation of the oxo intermediate, O−O bond formation proceeds through a binuclear mechanism in which the coupling of two *═O results in a *−O−O−* bridge.[29,55,121] In the bifunctional path, nucleophilic attack of H_2O or OH^- combines with transfer of a H^+/e^- to a hydrogen acceptor site A.[52,70,122]

Both mechanisms avoid formation of the *−OOH intermediate, which limits the overpotential of solid-state catalysts lying on the strong binding side of the volcano for the mononuclear mechanism.[47,68] Accordingly, negligible thermodynamic overpotentials for catalysts become possible (when the reaction proceeds through the bifunctional pathway)[70] (see the green dashed line in Figure 4). For molecular

DOI: 10.1021/acs.jpcc.8b03935
J. Phys. Chem. C 2018, 122, 12404−12412

electrocatalysts, the regime where the thermodynamics can be improved by altering the reaction mechanism still coincides with the weak binding side of the volcano. Thus, oxidation of *−OH to *═O determines the overpotential, and any changes to the O−O bond formation mechanism will not affect the overpotential. Accordingly, molecular catalysts do not benefit from avoiding the formation of the *−OOH intermediate.

CONCLUSIONS

In summary, we have demonstrated the existence of strong linear free energy scaling relationships between intermediates for the oxygen evolution reaction for molecular water oxidation catalysts that differ from those found in solid-state catalysts. Whereas the LFESRs strongly depend on the choice of density functional approximation, we have established accurate benchmark computations, which reveal a constant difference of 3.1 eV between *−OH and *−OOH. These findings agree well with the scaling relationships found for solid-state species. However, the energy difference between *−OH and *═O is found to be almost independent of the choice of catalyst, which results in significant changes to the overall shape of the volcano plot for molecular species. In contrast to heterogeneous electrocatalysts, the two slopes of the volcano no longer meet in a sharp "peak" at a *−OH binding energy of 1.6 eV. Rather, the top of the molecular volcano is characterized by a broad plateau encompassing binding energies ranging between 0.1 and 1.7 eV. In this range, an overpotential of approximately 0.3 eV, slightly lower than in the solid-state case, is expected. Overall, distinguishing features of the molecular volcano, namely, the large plateau and the somewhat higher top, imply that molecular water oxidation catalysts should generally be superior to heterogeneous catalysts when proceeding through the mononuclear mechanism. Taking into account the possible alternative reaction pathways that avoid the formation of *−OOH and thus formally allow for water oxidation at negligible overpotentials, the picture changes. Owing to the early transition to the "weak binding" regime where oxidation of H_2O to *═O is potential determining, these mechanisms no longer lower the overpotential for molecular or solid-state catalysts. Accordingly, solid-state catalysts should have lower overpotentials than those of their molecular counterparts if they are able to access alternative bifunctional reaction paths.

ASSOCIATED CONTENT

Supporting Information

The Supporting Information is available free of charge on the ACS Publications website at DOI: 10.1021/acs.jpcc.8b03935.

Construction of volcano plots, linear free energy scaling relationships, optimized structures, and benchmark computations (PDF)

AUTHOR INFORMATION

Corresponding Author

*E-mail: clemence.corminboeuf@epfl.ch.

ORCID

Michael Busch: 0000-0003-3883-2868

Alberto Fabrizio: 0000-0002-4440-3149

Clemence Corminboeuf: 0000-0001-7993-2879

Author Contributions

⊥M.B. and A.F. contributed equally to this work.

Notes

The authors declare no competing financial interest.

ACKNOWLEDGMENTS

The National Centre of Competence in Research (NCCR) "Materials' Revolution: Computational Design and Discovery of Novel Materials (MARVEL)" of the Swiss National Science Foundation (SNSF) and the EPFL are acknowledged for financial support.

REFERENCES

(1) Carmo, M.; Fritz, D.; Mergel, J.; Stolten, D. A Comprehensive Review on PEM Water Electrolysis. *Int. J. Hydrogen Energy* **2013**, *38*, 4901−4934.

(2) Greeley, J.; Markovic, N. The Road from Animal Electricity to Green Energy: Combining Experiment and Theory in Electrocatalysis. *Energy Environ. Sci.* **2012**, *5*, 9246−9256.

(3) Artero, V.; Fontecave, M.; Chavarot-Kerlidou, M. Splitting Water with Cobalt. *Angew. Chem., Int. Ed.* **2011**, *50*, 7238−7266.

(4) Kondratenko, E.; Mul, G.; Baltrusaitis, J.; Larrazábalc, G.; Pérez-Ramírez, J. Status and Perspectives of CO2 Conversion into Fuels and Chemicals by Catalytic, Photocatalytic and Electrocatalytic Processes. *Energy Environ. Sci.* **2013**, *6*, 3112−3135.

(5) Sahara, G.; Ishitani, O. Efficient Photocatalysts for CO2 Reduction. *Inorg. Chem.* **2015**, *54*, 5096−5104.

(6) Medina-Ramos, J.; Pupillo, R.; Keane, T.; DiMeglio, J.; Rosenthal, J. Efficient Conversion of CO2 to CO Using Tin and Other Inexpensive and Easily Prepared Post-Transition Metal Catalysts. *J. Am. Chem. Soc.* **2015**, *137*, 5021−5027.

(7) Liu, C.; Colón, B.; Ziesack, M.; Silver, P.; Nocera, D. Water Splitting-Biosynthetic System with CO2 Reduction Efficiencies Exceeding Photosynthesis. *Science* **2016**, *352*, 1210−1213.

(8) Marjolin, A.; Keith, J. Thermodynamic Descriptors for Molecules That Catalyze Efficient CO2 Electroreductions. *ACS Catal.* **2015**, *5*, 1123−1130.

(9) Birdja, Y.; Shen, J.; Koper, M. Influence of the Metal Center of Metalloprotoporphyrins on the Electrocatalytic CO2 Reduction to Formic Acid. *Catal. Today* **2017**, *288*, 37−47.

(10) Trasatti, S. Electrocatalysis: Understanding the Success of DSA. *Electrochim. Acta* **2000**, *45*, 2377−2385.

(11) Petrie, S.; Pace, R.; Stranger, R. Resolving the Differences Between the 1.9 and 1.95 Crystal Structures of PhotosystemII: A Single Proton Relocation Defines Two Tautomeric Forms of the Water-Oxidizing Complex. *Angew. Chem., Int. Ed.* **2015**, *54*, 7120−7124.

(12) Siegbahn, P. E. M. A Structure-Consistent Mechanism for Dioxygen Formation in Photosystem II. *Chem. - Eur. J.* **2008**, *14*, 8290−8302.

(13) Loll, B.; Kern, J.; Saenger, W.; Zouni, A.; Biesiadka, J. Towards Complete Cofactor Arrangement in the 3.0A Resolution Structure of Photosystem II. *Nature* **2005**, *438*, 1040−1044.

(14) Umena, Y.; Kawakami, K.; Shen, J.; Kamiya, N. Crystal Structure of Oxygen-Evolving Photosystem II at a Resolution of 1.9 Å. *Nature* **2011**, *473*, 55−61.

(15) Gersten, S. W.; Samuels, G. J.; Meyer, T. J. Catalytic Oxidation of Water by an Oxo-Bridged Ruthenium Dimer. *J. Am. Chem. Soc.* **1982**, *104*, 4029−4030.

(16) Blakemore, J. D.; Schley, N.; Balcells, D.; Hull, J.; Olack, G.; Incarvito, C.; Eisenstein, O.; Brudvig, G.; Crabtree, R. Half-Sandwich Iridium Complexes for Homogeneous Water-Oxidation Catalysis. *J. Am. Chem. Soc.* **2010**, *132*, 16017−16029.

(17) Hull, J. F.; Balcells, D.; Blakemore, J. D.; Incarvito, C. D.; Eisenstein, O.; Brudvig, G. W.; Crabtree, R. H. Highly Active and Robust Cp* Iridium Complexes for Catalytic Water Oxidation. *J. Am. Chem. Soc.* **2009**, *131*, 8730−8731.

(18) Blakemore, J. D.; Crabtree, R.; Brudvig, G. Molecular Catalysts for Water Oxidation. *Chem. Rev.* **2015**, *115*, 12974−13005.

DOI: 10.1021/acs.jpcc.8b03935
J. Phys. Chem. C 2018, 122, 12404−12412

(19) Wang, L.; Duan, L.; Stewart, B.; Pu, M.; Liu, J.; Privalov, T.; Sun, L. Toward Controlling Water Oxidation Catalysis: Tunable Activity of Ruthenium Complexes with Axial Imidazole/DMSO Ligands. *J. Am. Chem. Soc.* **2012**, *134*, 18868−18880.
(20) Rabten, W.; Kärkäs, M.; Åkermark, T.; Chen, H.; Liao, R.; Tinnis, F.; Sun, J.; Siegbahn, P.; Andersson, P.; Åkermark, B. Catalytic Water Oxidation by a Molecular Ruthenium Complex: Unexpected Generation of a Single-Site Water Oxidation Catalyst. *Inorg. Chem.* **2015**, *54*, 4611−4620.
(21) Younus, H. A.; Ahmad, N.; Chughtai, A.; Vandichel, M.; Busch, M.; Van Hecke, K.; Yusubov, M.; Song, S.; Verpoort, F. A Robust Molecular Catalyst Generated In-Situ for Photo- and Electrochemical Water Oxidation. *ChemSusChem* **2017**, *10*, 862−875.
(22) Hodel, F.; Luber, S. What Influences the Water Oxidation Activity of a Bioinspired Molecular CoII4O4 Cubane? an In-Depth Exploration of Catalytic Pathways. *ACS Catal.* **2016**, *6*, 1505−1517.
(23) Schilling, M.; Patzke, G. R.; Hutter, J.; Luber, S. Computational Investigation and Design of Cobalt Aqua Complexes for Homogeneous Water Oxidation. *J. Phys. Chem. C* **2016**, *120*, 7966−7975.
(24) Young, K. J.; Takase, M.; Brudvig, G. An Anionic N-Donor Ligand Promotes Manganese-Catalyzed Water Oxidation. *Inorg. Chem.* **2013**, *52*, 7615−7622.
(25) Limburg, J.; Vrettos, J. S.; Chen, H.; de Paula, J. C.; Crabtree, R. H.; Brudvig, G. W. Characterization of the O2-Evolving Reaction Catalyzed by [(terpy)(H2O) MnIII (O) 2MnIV (OH2)(terpy)]-(NO3) 3 (terpy = 2, 2′: 6, 2″-Terpyridine). *J. Am. Chem. Soc* **2001**, *123*, 423−430.
(26) Liao, R.; Kärkäs, M.; Lee, B.; Åkermark, B.; Siegbahn, P. Photosystem II like Water Oxidation Mechanism in a Bioinspired Tetranuclear Manganese Complex. *Inorg. Chem.* **2015**, *54*, 342−351.
(27) Yagi, M.; Kaneko, M. Molecular Catalysts for Water Oxidation. *Chem. Rev.* **2001**, *101*, 21−36.
(28) Ruettinger, W.; Yagi, M.; Wolf, K.; Bernasek, S.; Dismukes, G. C. O2 Evolution from the Manganese-Oxo Cubane Core Mn4O4 6+: A Molecular Mimic of the Photosynthetic Water Oxidation Enzyme? *J. Am. Chem. Soc.* **2000**, *122*, 10353−10357.
(29) Busch, M.; Ahlberg, E.; Panas, I. Electrocatalytic Oxygen Evolution from Water on a Mn(III-V) Dimer Model Catalyst - a DFT Perspective. *Phys. Chem. Chem. Phys.* **2011**, *13*, 15069−15076.
(30) Rivalta, I.; Yang, K.; Brudvig, G.; Batista, V. Triplet Oxygen Evolution Catalyzed by a Biomimetic Oxomanganese Complex: Functional Role of the Carboxylate Buffer. *ACS Catal.* **2015**, *5*, 2384−2390.
(31) Fillol, J. L.; Codolà, Z.; Garcia-Bosch, I.; Gómez, L.; Pla, J. J.; Costas, M. Efficient Water Oxidation Catalysts Based on Readily Available Iron Coordination Complexes. *Nat. Chem.* **2011**, *3*, 807−813.
(32) Ertem, M. Z.; Gagliardi, L.; Cramer, C. J. Quantum Chemical Characterization of the Mechanism of an Iron-Based Water Oxidation Catalyst. *Chem. Sci.* **2012**, *3*, 1293.
(33) Codolà, Z.; Garcia-Bosch, I.; Acuña-Parés, F.; Prat, I.; Luis, J. M.; Costas, M.; Lloret-Fillol, J. Electronic Effects on Single-Site Iron Catalysts for Water Oxidation. *Chem. - Eur. J.* **2013**, *19*, 8042−8047.
(34) Coggins, M. K.; Zhang, M. T.; Vannucci, A. K.; Dares, C. J.; Meyer, T. J. Electrocatalytic Water Oxidation by a Monomeric Amidate-Ligated Fe(III)-Aqua Complex. *J. Am. Chem. Soc.* **2014**, *136*, 5531−5534.
(35) Liao, R.-Z.; Li, X.-C.; Siegbahn, P. E. M. Reaction Mechanism of Water Oxidation Catalyzed by Iron Tetraamido Macrocyclic Ligand Complexes - a DFT Study. *Eur. J. Inorg. Chem.* **2014**, *2014*, 728−741.
(36) Das, B.; Orthaber, A.; Ott, S.; Thapper, A. Iron Pentapyridyl Complexes As Molecular Water Oxidation Catalysts: Strong Influence of a Chloride Ligand and PH in Altering the Mechanism. *ChemSusChem* **2016**, *9*, 1178−1186.
(37) Bernasconi, L.; Kazaryan, A.; Belanzoni, P.; Baerends, E. J. Catalytic Oxidation of with High-Spin Iron(IV)-Oxo Species: Role of the Water Solvent. *ACS Catal.* **2017**, *7*, 4018−4025.
(38) Zhang, M.; Zhang, M. T.; Hou, C.; Ke, Z. F.; Lu, T. B. Homogeneous Electrocatalytic Water Oxidation at Neutral PH by a Robust Macrocyclic Nickel(II) Complex. *Angew. Chem., Int. Ed.* **2014**, *53*, 13042−13048.
(39) Han, Y.; Wu, Y.; Lai, W.; Cao, R. Electrocatalytic Water Oxidation by a Water-Soluble Nickel Porphyrin Complex at Neutral Ph with Low Overpotential. *Inorg. Chem.* **2015**, *54*, 5604−5613.
(40) Luo, G. Y.; Huang, H. H.; Wang, J. W.; Lu, T. B. Further Investigation of a Nickel-Based Homogeneous Water Oxidation Catalyst with Two Cis Labile Sites. *ChemSusChem* **2016**, *9*, 485−491.
(41) Wang, J.-W.; Zhang, X.-Q.; Huang, H.-H.; Lu, T.-B. A Nickel(II) Complex As a Homogeneous Electrocatalyst for Water Oxidation at Neutral PH: Dual Role of HPO 4 2 in Catalysis. *ChemCatChem* **2016**, *8*, 3287−3293.
(42) Barnett, S. M.; Goldberg, K. I.; Mayer, J. M. A Soluble Copper-Bipyridine Water-Oxidation Electrocatalyst. *Nat. Chem.* **2012**, *4*, 498−502.
(43) Zhang, M. T.; Chen, Z.; Kang, P.; Meyer, T. J. Electrocatalytic Water Oxidation with a Copper(II) Polypeptide Complex. *J. Am. Chem. Soc.* **2013**, *135*, 2048−2051.
(44) Zhang, T.; Wang, C.; Liu, S.; Wang, J. L.; Lin, W. A Biomimetic Copper Water Oxidation Catalyst with Low Overpotential. *J. Am. Chem. Soc.* **2014**, *136*, 273−281.
(45) Zhang, M.; de Respinis, M.; Frei, H. Time-Resolved Observations of Water Oxidation Intermediates on a Cobalt Oxide Nanoparticle Catalyst. *Nat. Chem.* **2014**, *6*, 362−367.
(46) Jiao, F.; Frei, H. Nanostructured Cobalt Oxide Clusters in Mesoporous Silica As Efficient Oxygen-Evolving Catalysts. *Angew. Chem., Int. Ed.* **2009**, *48*, 1841−1844.
(47) Man, I. C.; Su, H.; Calle-Vallejo, F.; Hansen, H. A.; Martìnez, N. G.; Inoglu, J. I.; Kitchin, J.; Jaramillo, T. F.; Nørskov, J. K.; Rossmeisl, J. Universality in Oxygen Evolution Electrocatalysis on Oxide Surfaces. *ChemCatChem.* **2011**, *3*, 1159−1165.
(48) Busch, M.; Ahlberg, E.; Panas, I. Validation of Binuclear Descriptor for Mixed Transition Metal Oxide Supported Electrocatalytic Water Oxidation. *Catal. Today* **2013**, *202*, 114−119.
(49) Busch, M.; Ahlberg, E.; Panas, I. Hydroxide Oxidation and Peroxide Formation at Embedded Binuclear Transition Metal Sites; TM = Cr, Mn, Fe, Co. *Phys. Chem. Chem. Phys.* **2011**, *13*, 15062−15068.
(50) Chou, N. H.; Ross, P. N.; Bell, A. T.; Tilley, T. D. Comparison of Cobalt-Based Nanoparticles As Electrocatalysts for Water Oxidation. *ChemSusChem* **2011**, *4*, 1566−1569.
(51) Bajdich, M.; García-Mota, M.; Vojvodic, A.; Nørskov, J.; Bell, A. Theoretical Investigation of the Activity of Cobalt Oxides for the Electrochemical Oxidation of Water. *J. Am. Chem. Soc.* **2013**, *135*, 13521−13530.
(52) Frydendal, R.; Busch, M.; Halck, N.; Paoli, E.; Krtil, P.; Chorkendorff, I.; Rossmeisl, J. Enhancing Activity for the Oxygen Evolution Reaction: The Beneficial Interaction of Gold with Manganese and Cobalt Oxides. *ChemCatChem* **2015**, *7*, 149−154.
(53) El-Deab, M. S.; Awad, M. I.; Mohammad, A. M.; Ohsaka, T. Enhanced Water Electrolysis: Electrocatalytic Generation of Oxygen Gas at Manganese Oxide Nanorods Modified Electrodes. *Electrochem. Commun.* **2007**, *9*, 2082−2087.
(54) Mohammad, A. M.; Awad, M. I.; El-Deab, M. S.; Okajima, T.; Ohsaka, T. Electrocatalysis by Nanoparticles: Optimization of the Loading Level and Operating PH for the Oxygen Evolution at Crystallographically Oriented Manganese Oxide Nanorods Modified Electrodes. *Electrochim. Acta* **2008**, *53*, 4351−4358.
(55) Busch, M.; Ahlberg, E.; Panas, I. Water Oxidation on MnO_x and IrO_x: Why Similar Performance? *J. Phys. Chem. C* **2013**, *117*, 288−292.
(56) Limburg, J.; Brudvig, G. W.; Crabtree, R. H. O2 Evolution and Permanganate Formation from High-Valent Manganese Complexes. *J. Am. Chem. Soc.* **1997**, *119*, 2761−2762.
(57) Calle-Vallejo, F.; Martínez, J.; García-Lastra, J.; Rossmeisl, J.; Koper, M. Physical and Chemical Nature of the Scaling Relations Between Adsorption Energies of Atoms on Metal Surfaces. *Phys. Rev. Lett.* **2012**, *108*, No. 116103.

DOI: 10.1021/acs.jpcc.8b03935
J. Phys. Chem. C 2018, 122, 12404−12412

(58) Busch, M.; Wodrich, M.; Corminboeuf, C. Linear Scaling Relationships and Volcano Plots in Homogeneous Catalysis - Revisiting the Suzuki Reaction. *Chem. Sci.* **2015**, *6*, 6754−6761.
(59) Abild-Pedersen, F.; Greeley, J.; Studt, F.; Rossmeisl, J.; Munter, T.; Moses, P.; Skúlason, E.; Bligaard, T.; Nørskov, J. Scaling Properties of Adsorption Energies for Hydrogen-Containing Molecules on Transition-Metal Surfaces. *Phys. Rev. Lett.* **2007**, *99*, No. 016105.
(60) Gerischer, H. Mechanismus Der Elektrolytischen Wasserstoffabscheidung Und Adsorptionsenergie Von Atomarem Wasserstoff. *Bull. Soc. Chim. Belg.* **1958**, *67*, 506−527.
(61) Parsons, R. The Rate of Electrolytic Hydrogen Evolution and the Heat of Adsorption of Hydrogen. *Trans. Faraday Soc.* **1958**, *54*, 1053−1063.
(62) Nørskov, J. K.; Bligaard, T.; Rossmeisl, J.; Christensen, C. Towards the Computational Design of Solid Catalysts. *Nat. Chem.* **2009**, *1*, 37−46.
(63) Sabatier, P. Hydrogénations et Déshydrogénations Par Catalyse. *Ber. Dtsch. Chem. Ges.* **1911**, *44*, 1984−2001.
(64) Sabatier, P. *La Catalyse En Chimie Organique*; Librairie Polytechnique: Paris, 1913.
(65) Kozuch, S.; Shaik, S. How to Conceptualize Catalytic Cycles? the Energetic Span Model. *Acc. Chem. Res.* **2011**, *44*, 101−110.
(66) Kozuch, S. *Understanding Organometallic Reaction Mechanisms and Catalysis: Computational and Experimental Tools*; Ananikov, V. P., Ed.; 2014; pp 1−383.
(67) Swiegers, G. F. *Mechanical Catalysis: Methods of Enzymatic, Homogeneous, and Heterogeneous Catalysis*; John Wiley & Sons, 2008; pp 1−351.
(68) Koper, M. T. M. Thermodynamic Theory of Multi-Electron Transfer Reactions: Implications for Electrocatalysis. *J. Electroanal. Chem.* **2011**, *660*, 254−260.
(69) Wodrich, M.; Busch, M.; Corminboeuf, C. Accessing and Predicting the Kinetic Profiles of Homogeneous Catalysts from Volcano Plots. *Chem. Sci.* **2016**, *7*, 5723−5735.
(70) Busch, M.; Halck, N.; Kramm, U.; Siahrostami, S.; Krtil, P.; Rossmeisl, J. Beyond the Top of the Volcano? - a Unified Approach to Electrocatalytic Oxygen Reduction and Oxygen Evolution. *Nano Energy* **2016**, *29*, 126−135.
(71) Calle-Vallejo, F.; Martínez, I.; Rossmeisl, J. Density Functional Studies of Functionalized Graphitic Materials with Late Transition Metals for Oxygen Reduction Reactions. *Phys. Chem. Chem. Phys.* **2011**, *13*, 15639−15643.
(72) Dogutan, D. K.; McGuire, R., Jr.; Nocera, D. G. Electocatalytic Water Oxidation by Cobalt(III) Hangman β -Octafluoro Corroles. *J. Am. Chem. Soc.* **2011**, *133*, 9178−9180.
(73) Zhang, W.; Lai, W.; Cao, R. Energy-Related Small Molecule Activation Reactions: Oxygen Reduction and Hydrogen and Oxygen Evolution Reactions Catalyzed by Porphyrin- and Corrole-Based Systems. *Chem. Rev.* **2017**, *117*, 3717−3797.
(74) Tao, J.; Perdew, P.; Staroverov, V. N.; Scuseria, G. E. Climbing the Density Functional Ladder: Nonempirical Meta-Generalized Gradient Approximation Designed for Molecules and Solids. *Phys. Rev. Lett.* **2003**, *91*, No. 146401.
(75) Grimme, S.; Antony, J.; Ehrlich, S.; Krieg, H. Consistent and Accurate Ab Initio Parametrization of Density Functional Dispersion Correction (DFT-D) for the 94 Elements H-Pu. *J. Chem. Phys.* **2010**, *132*, No. 154104.
(76) Weigend, F.; Ahlrichs, R. Balanced Basis Sets of Split Valence, Triple Zeta Valence and Quadruple Zeta Valence Quality for H to Rn: Design and Assessment of Accuracy. *Phys. Chem. Chem. Phys.* **2005**, *7*, 3297−305.
(77) Scalmani, G.; Frisch, M. Continuous Surface Charge Polarizable Continuum Models of Solvation. I. General Formalism. *J. Chem. Phys.* **2010**, *132*, No. 114110.
(78) Mennucci, B.; Cammi, R.; Tomasi, J. Excited States and Solvatochromic Shifts Within a Nonequilibrium Solvation Approach: A New Formulation of the Integral Equation Formalism Method at the Self-Consistent Field, Configuration Interaction, and Multiconfiguration Self-Consistent Field Level. *J. Chem. Phys.* **1998**, *109*, 2798−2807.
(79) Rossmeisl, J.; Qu, Z.; Zhu, H.; Kroes, G.; Nørskov, J. K. Electrolysis of Water on Oxide Surfaces. *J. Electroanal. Chem.* **2007**, *607*, 83−99.
(80) Rossmeisl, J.; Logadottir, A.; Nørskov, J. K. Electrolysis of Water on (oxidized) Metal Surfaces. *Chem. Phys.* **2005**, *319*, 178−184.
(81) Gritsenko, O.; Schipper, P.; Baerends, E. Exchange and Correlation Energy in Density Functional Theory: Comparison of Accurate Density Functional Theory Quantities with Traditional Hartree-Fock Based Ones and Generalized Gradient Approximations for the Molecules Li2, N2. *J. Chem. Phys.* **1997**, *107*, 5007.
(82) Grimme, S. Semiempirical GGA-Type Density Functional Constructed with a Long-Range Dispersion Correction. *J. Comput. Chem.* **2006**, *27*, 1787−1799.
(83) Becke, A. D. Density-Functional Exchange-Energy Approximation with Correct Asymptotic Behavior. *Phys. Rev. A* **1988**, *38*, 3098−3100.
(84) Lee, C.; Yang, W.; Parr, R. G. Development of the Colle-Salvetti Correlation-Energy Formula into a Functional of the Electron Density. *Phys. Rev. B* **1988**, *37*, 785−789.
(85) Perdew, J. Density-Functional Approximation for the Correlation Energy of the Inhomogeneous Electron Gas. *Phys. Rev. B* **1986**, *33*, 8822−8824.
(86) Perdew, J. P.; Burke, K.; Ernzerhof, M. Generalized Gradient Approximation Made Simple. *Phys. Rev. Lett.* **1996**, *77*, 3865−3868.
(87) Perdew, J. P.; Burke, K.; Ernzerhof, M. Erratum: Generalized Gradient Approximation Made Simple. *Phys. Rev. Lett.* **1997**, *78*, No. 1396.
(88) Zhao, Y.; Truhlar, D. G. A New Local Density Functional for Main-Group Thermochemistry, Transition Metal Bonding, Thermochemical Kinetics, and Noncovalent Interactions. *J. Chem. Phys.* **2006**, *125*, No. 194101.
(89) Becke, A. D. Density-Functional Thermochemistry. III. the Role of Exact Exchange. *J. Chem. Phys.* **1993**, *98*, 5648−5652.
(90) Devlin, F. J.; Finley, J. W.; Stephens, P. J.; Frisch, M. J. Ab-Initio Calculation of Vibrational Absorption and Circular-Dichroism Spectra Using Density-Functional Force-Fields - a Comparison of Local, Nonlocal, and Hybrid Density Functionals. *J. Phys. Chem.* **1995**, *99*, 16883−16902.
(91) Perdew, J. P.; Chevary, J.; Vosko, S.; Jackson, K.; Pederson, M.; Singh, D.; Fiolhais, C. Atoms, Molecules, Solids, and Surfaces: Applications of the Generalized Gradient Approximation for Exchange and Correlation. *Phys. Rev. B* **1992**, *46*, 6671−6687.
(92) Adamo, C.; Barone, V. Exchange Functionals with Improved Long-Range Behavior and Adiabatic Connection Methods Without Adjustable Parameters: The MPW and MPW1PW Models. *J. Chem. Phys.* **1998**, *108*, 664−675.
(93) Austin, A.; Petersson, G.; Frisch, M.; Dobek, F.; Scalmani, G.; Throssell, K. A Density Functional with Spherical Atom Dispersion Terms. *J. Chem. Theory Comput.* **2012**, *8*, 4989−5007.
(94) Adamo, C.; Barone, V. Toward Reliable Density Functional Methods Without Adjustable Parameters: The PBE0 Model. *J. Chem. Phys.* **1999**, *110*, 6158.
(95) Ernzerhof, M.; Scuseria, G. Assessment of the Perdew-Burke-Ernzerhof Exchange-Correlation Functional. *J. Chem. Phys.* **1999**, *110*, 5029.
(96) Becke, A. A New Mixing of Hartree-Fock and Local Density-Functional Theories. *J. Chem. Phys.* **1993**, *98*, 1372.
(97) Zhao, Y.; Truhlar, D. The M06 Suite of Density Functionals for Main Group Thermochemistry, Thermochemical Kinetics, Noncovalent Interactions, Excited States, and Transition Elements: Two New Functionals and Systematic Testing of Four M06-Class Functionals and 12 Other Functionals. *Theor. Chem. Acc.* **2008**, *120*, 215−241.
(98) Boese, A. D.; Martin, J. Development of Density Functional for Thermochemical Kinetics. *J. Chem. Phys.* **2004**, *121*, 3405−3416.
(99) Zhao, Y.; Truhlar, D. Comparative DFT Study of Van Der Waals Complexes: Rare-Gas Dimers, Alkaline-Earth Dimers, Zinc Dimer and Zinc-Rare-Gas Dimers. *J. Phys. Chem. A* **2006**, *110*, 5121−5129.

DOI: 10.1021/acs.jpcc.8b03935
J. Phys. Chem. C 2018, 122, 12404−12412

(100) Zhao, Y.; Truhlar, D. Density Functional for Spectroscopy: No Long-Range Self-Interaction Error, Good Performance for Rydberg and Charge-Transfer States, and Better Performance on Average Than B3LYP for Ground States. *J. Phys. Chem. A* **2006**, *110*, 13126−13130.
(101) Vydrov, O. A.; Heyd, J.; Krukau, A.; Scuseria, G. Importance of Short-Range Versus Long-Range Hartree-Fock Exchange for the Performance of Hybrid Density Functionals. *J. Chem. Phys.* **2006**, *125*, No. 074106.
(102) Vydrov, O. A.; Scuseria, G. Assessment of a Long-Range Corrected Hybrid Functional. *J. Chem. Phys.* **2006**, *125*, No. 234109.
(103) Vydrov, O. A.; Scuseria, G.; Perdew, J. Tests of Functionals for Systems with Fractional Electron Number. *J. Chem. Phys.* **2007**, *126*, No. 154109.
(104) Chai, J. D.; Head-Gordon, M. Long-Range Corrected Hybrid Density Functionals with Damped Atom-atom Dispersion Corrections. *Phys. Chem. Chem. Phys.* **2008**, *10*, 6615−6620.
(105) Yanai, T.; Tew, D.; Handy, N. A New Hybrid Exchange-Correlation Functional Using the Coulomb-Attenuating Method (CAM-B3LYP). *Chem. Phys. Lett.* **2004**, *393*, 51−57.
(106) Frisch, M.; Trucks, G.; Schlegel, H.; Scuseria, G.; Robb, M.; Cheeseman, J.; Scalmani, G.; Barone, V.; Mennucci, B.; Petersson, G.; et al. *Gaussian 09*, revision D.01; Gaussian Inc.: Wallingford CT, 2009.
(107) Ebisuzaki, R.; Watanabe, Y.; Nakano, H. Efficient Implementation of Relativistic and Non-Relativistic Quasidegenerate Perturbation Theory with General Multiconfigurational Reference Functions. *Chem. Phys. Lett.* **2007**, *442*, 164−169.
(108) Nakano, H.; Uchiyama, R.; Hirao, K. Quasi-Degenerate Perturbation Theory with General Multiconfiguration Self-Consistent Field Reference Functions. *J. Comput. Chem.* **2002**, *23*, 1166−1175.
(109) Schmidt, M.; Baldridge, K.; Boatz, J.; Elbert, S.; Gordon, J.; Jensen, J.; Koseki, S.; Matsunaga, N.; Nguyen, K.; Su, S.; et al. General Atomic and Molecular Electronic Structure System. *J. Comput. Chem.* **1993**, *14*, 1347−1363.
(110) Vojvodic, A.; Calle-Vallejo, F.; Guo, W.; Wang, S.; Toftelund, A.; Studt, F.; Martinez, J. I.; Shen, J.; Man, I. C.; Rossmeisl, J.; et al. On the Behavior of Brønsted-Evans-Polanyi Relations for Transition Metal Oxides. *J. Chem. Phys.* **2011**, *134*, No. 244509.
(111) Busch, M.; Wang, R.; Hellman, A.; Rossmeisl, J.; Grönbeck, H. The Influence of Inert Ions on the Reactivity of Manganese Oxides. *J. Phys. Chem. C* **2018**, *122*, 216−226.
(112) Xu, Z.; Rossmeisl, J.; Kitchin, J. A Linear Response DFT+U Study of Trends in the Oxygen Evolution Activity of Transition Metal Rutile Dioxides. *J. Phys. Chem. C* **2015**, *119*, 4827−4833.
(113) Christensen, R.; Hansen, H.; Dickens, C.; Nørskov, J.; Vegge, T. Functional Independent Scaling Relation for ORR/OER Catalysts. *J. Phys. Chem. C* **2016**, *120*, 24910−24916.
(114) Calle-Vallejo, F.; Krabbe, A.; García-Lastra, J. How Covalence Breaks Adsorption-Energy Scaling Relations and Solvation Restores Them. *Chem. Sci.* **2017**, *8*, 124−130.
(115) Jannuzzi, S. A. V.; Phung, Q.; Domingo, A.; Formiga, A.; Pierloot, K. Spin State Energetics and Oxyl Character of Mn-Oxo Porphyrins by Multiconfigurational Ab Initio Calculations: Implications on Reactivity. *Inorg. Chem.* **2016**, *55*, 5168−5179.
(116) Radoń, M.; Broclawik, E.; Pierloot, K. DFT and Ab Initio Study of Iron-Oxo Porphyrins: May They Have a Low-Lying Iron(V)-Oxo Electromer? *J. Chem. Theory Comput.* **2011**, *7*, 898−908.
(117) Chen, H.; Lai, W.; Shaik, S. Multireference and Multiconfiguration Ab Initio Methods in Heme-Related Systems: What Have We Learned So Far? *J. Phys. Chem. B* **2011**, *115*, 1727−1742.
(118) Ghosh, A.; Taylor, P. R. High-Level Ab Initio Calculations on the Energetics of Low-Lying Spin States of Biologically Relevant Transition Metal Complexes: A First Progress Report. *Curr. Opin. Chem. Biol.* **2003**, *7*, 113−124.
(119) Berryman, V. E. J.; Boyd, R. J.; Johnson, E. R. Balancing Exchange Mixing in Density-Functional Approximations for Iron Porphyrin. *J. Chem. Theory Comput.* **2015**, *11*, 3022−3028.
(120) Wodrich, M.; Sawatlon, B.; Busch, M.; Corminboeuf, C. On the Generality of Molecular Volcano Plots. *ChemCatChem* **2018**, *10*, 1−7.
(121) Bockris, J. O.; Otagawa, T. Mechanism of Oxygen Evolution on Perovskites. *J. Phys. Chem.* **1983**, *87*, 2960−2971.
(122) Halck, N. B.; Petrykin, V.; Krtil, P.; Rossmeisl, J. Beyond the Volcano Limitations in Electrocatalysis - Oxygen Evolution Reaction. *Phys. Chem. Chem. Phys.* **2014**, *16*, 13682−13688.

DOI: 10.1021/acs.jpcc.8b03935
J. Phys. Chem. C 2018, 122, 12404−12412